CMS Draft Analysis Note

The content of this note is intended for CMS internal use and distribution only

Searching for exclusively produced top quark pairs

B. Ribeiro Lopes[2], P. Silva[1], J. Hollar[2], and M. Gallinaro[2]

[1] CERN, Geneva, Switzerland
[2] LIP, Laboratório de Instrumentação e Física Experimental de Partículas, Lisbon, Portugal

Abstract

A search for exclusive production of top quark pairs, where the outgoing unfragmented protons are detected about 210 m away from the centre of the CMS detector, is described. Proton-proton collision data at $\sqrt{s} =$13 TeV collected in 2017 are used for the search. An upper limit is set on the production cross section.

Contents

1 Introduction

This note reports on the search for exclusive top quark pairs, $pp \rightarrow p t\bar{t} p$, where the $t\bar{t}$ pair decays dileptonically. The process is represented by the Feynman diagrams in Fig. 1. If identified in the data, this production channel is characterized by the suppression of additional radiation in the central region. If the kinematics of the protons are measured, it offers the possibility of determining the $t\bar{t}$ production threshold with a better resolution than the one that can be attained based on the inclusive production, through the reconstruction of the final states. The standard model (SM) prediction for the exclusive top pair production cross section is extremely small, $\mathcal{O}(1\,\text{fb})$ for photo-production, and it lacks updated predictions [1]. However, if new physics is present, the small cross section can be significantly enhanced either in the production of $t\bar{t}$ or in the production of similar final states containing at least two leptons [2–5].

In our analysis, the two leptons (electrons or muons) and the b-jets from the top quark decay are measured in the central CMS apparatus, while the two outgoing protons are measured in the Precision Proton Spectrometer (PPS). The latter is a near-beam magnetic spectrometer that uses the LHC magnets between the Interaction Point (IP) and detector stations at $\approx \pm 210$ m from the IP. Protons that have lost a small fraction of their momentum are bent out of the beam envelope so that their trajectories can be measured. The detectors that form PPS are called Roman Pots (RPs).
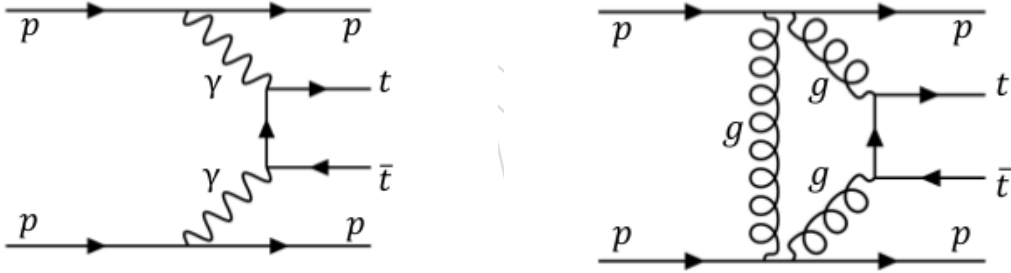

Figure 1: Exclusive $t\bar{t}$ production diagrams, via $\gamma\gamma$ fusion (left) and gg fusion (right).

2 Data and simulation samples

The analysis is performed using proton-proton collision data at $\sqrt{s} = 13$ TeV collected in 2017. The SingleMuon and SingleElectron primary datasets (PDs) are used[1]. The events passing the triggers listed on Table 1 are considered in our analysis. The total integrated luminosity corresponds to 41.4 fb^{-1}.

For the correlation between the central detector and the PPS, only data collected before Technical Stop 2 (TS2) are used. This is because both the detector efficiency and the PPS acceptance (due to new LHC optics) are different after-TS2 data and their measurement is still being finalized. In the PPS, RPs are identified followed by a 3-digit number, where the first digit is either 0 or 1 according to which arm the pot belongs to (0 for a positive z coordinate: z+, and 1 for negative z coordinate: z-), the second digit is the station number (either 0 for strips, or 2 for pixels), and the third is the RP number. RP numbered 003 and 103 contain silicon strip

---

[1]These are chosen as the starting point for the analysis, but could be complemented in a future version with the DoubleElectron, DoubleMuon and MuEG datasets to maximize the efficiency for the dilepton final state.

Table 1: Triggers used in the selection of the events. Events where both the muon and one of the electron trigger fires are allowed only if they are found in the SingleMuon PD.

Trigger name
HLT_Ele35_eta2p1_WPTight_Gsf_v*
HLT_Ele28_eta2p1_WPTight_Gsf_HT150_v*
HLT_Ele30_eta2p1_WPTight_Gsf_CentralPFJet35_EleCleaned_v*
HLT_IsoMu27_v

45 detectors, while those labeled 023 and 123 contain 3D pixel detectors. The scheme of the PPS
46 detector and its arms is shown in Fig. 2. Only data from RPs 003, 023, 103 and 123 were used,
47 since no alignment parameters exist for other RPs. Besides, only collisions with crossing angle
48 of 120, 130 or 140 μrad are considered, because there are no dispersion values available for
49 other crossing angles. The total integrated luminosity where combined CMS(central)-PPS data
50 have been analysed with calibrated pixels is thus reduced to 18.7 fb^{-1}.

Figure 2: Scheme of the PPS detectors used in the analysis.

51 The official Monte Carlo production samples have been used for the background. The name of
52 the samples and the cross section used to normalize them is summarized in Table 2.

Table 2: MC samples from the RunIIFall17MiniAOD-94X_mc2017_realistic_v10 production used in this analysis and their cross section.

Process	σ [pb]	MC sample
$t\bar{t}$	832	TTJets_TuneCP5_13TeV-amcatnloFXFX-pythia8
ZZ$\to 2\ell 2\nu$	0.564	ZZTo2L2Nu_13TeV_powheg_pythia8
WZ	47.13	WZ_TuneCP5_13TeV-pythia8
WW$\to 2\ell 2\nu$	12.178	WWTo2L2Nu_NNPDF31_TuneCP5_13TeV-powheg-pythia8
W+3 jets	942.3	W3JetsToLNu_TuneCP5_13TeV-madgraphMLM-pythia8
W+4 jets	524.2	W4JetsToLNu_TuneCP5_13TeV-madgraphMLM-pythia8
$\bar{t}$W	35.85	ST_tW_antitop_5f_NoFullyHadronicDecays_TuneCP5_13TeV-powheg-pythia8
tW	35.85	ST_tW_top_5f_NoFullyHadronicDecays_TuneCP5_13TeV-powheg-pythia8
DY (M>50 GeV)	5765.4	DYJetsToLL_M-50_TuneCP5_13TeV-amcatnloFXFX-pythia8

53 In addition, a signal $pp \to p\gamma\gamma p \to p t\bar{t} p$ sample was produced privately using FPMC [6] as
54 the matrix element generator and HERWIG++ [7] as the parton shower. This sample is used to
55 compute the acceptance and guide the final event selection.

56 **3 Event selection**

57 **3.1 Central detector selection**

58 Two charged leptons (electron or muon) with $M_{\ell\ell} > 20$ GeV are required. At least one of the
59 leptons is required to have $p_T > 30$ GeV, while the second one is required to have $p_T > 15$ GeV.
60 Both leptons are required to be reconstructed within $|\eta| < 2.5$. Depending on the flavour

and invariant mass of the dilepton system, the events are classified in the following exclusive categories:

- same-flavour leptons (*ee* or *μμ*) with reconstructed $m_{\ell\ell}$ around the Z mass ($m_{\ell\ell} \in$ [76, 106] GeV): Z-control region (CR);

- same-flavour (SF) leptons outside the Z-peak region: SF region;

- opposite-flavour (OF) leptons (*eμ*): OF region.

After categorizing the events, the following selection is applied:

- ≥ 1 jet ($p_T > 20$ GeV, $|\eta| < 4.7$ passing a "loose" pileup jet id criteria [8]);

- ≥ 1 b-jet ($p_T > 30$ GeV, $|\eta| < 2.5$ passing the deepCSV "medium" working point [9]);

- at least one "lepton-b jet" combination satisfies $M_{\ell b} < 160$ GeV.

In the last requirement, $m_{\ell b}$ refers to the invariant mass of lepton-b jet system. All lepton-b jet combinations are used and the one with the smallest $m_{\ell b}$ value is considered for the final selection. The criterion stems from the fact that, by energy conservation, one expects at leading order (LO), that $m_{\ell b} < \sqrt{m_t^2 - m_W^2} \approx 160$ GeV for $m_t = 172.5$ GeV and $m_W = 80.4$ GeV [10]. Thus, by applying such requirement, we expect that higher $t\bar{t}$ purity is attained.

Figure 3 shows the distribution of the invariant mass of the dilepton system for the SF and OF categories. It can be observed that even after removing the Z-peak region, the SF category is expected to be dominated by the Drell-Yan (DY) production. The excess in data for $m_{\ell\ell} < 50$ GeV is expected given the DY simulation does not include that region. For the OF category an overall excess is observed which may be attributed to missing simulated processes (to be checked).
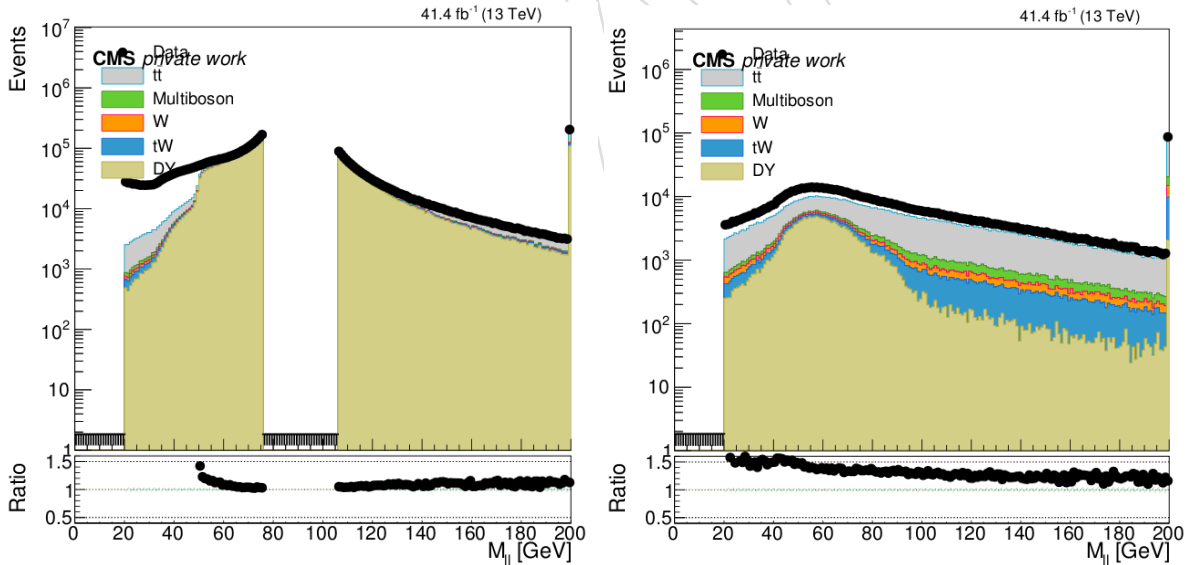

Figure 3: Control sample (central detector only): Distribution of the mass of the dilepton system after selecting two leptons for same-flavour (SF) leptons for events outside the Z peak (left), and for opposite-flavour leptons (right). Data are compared to the stacked predictions based on the simulation. The bottom panels show the ratio of the data to the total expected predictions.

Figure 4 shows the distribution of the b-tagging multiplicity. An excess is observed for events with low multiplicity in both the SF and OF categories. The excess disappears once the high purity region of $t\bar{t}$ is selected (≥ 1 b-tag).
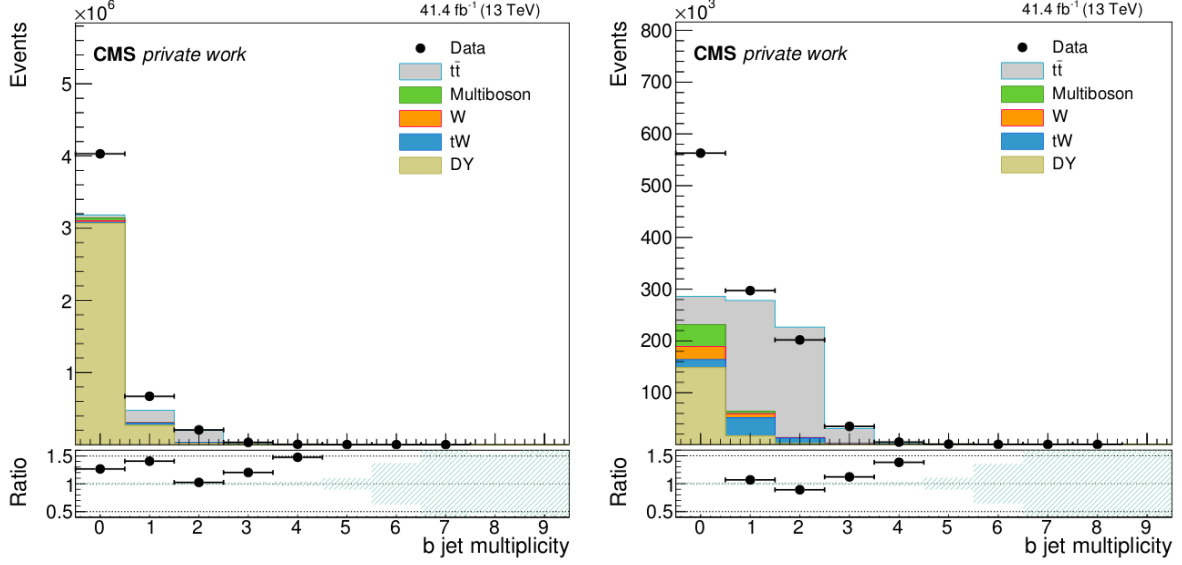
Figure 4: Control sample (central detector only): Number of b-tagged jets after requiring 2 leptons, for same flavour leptons except events under the Z peak (left) and for opposite flavour leptons (right).

Figure 5 shows the distribution of the $m_{\ell b}$ variable after the selection of at least 1 b-jet. An overall excess for the high $m_{\ell b}$ region is observed in both the SF and OF categories. This may be due to missing simulated samples (to be confirmed). In any case these events are removed from our analysis as the low $m_{\ell b}$ region ($m_{\ell b} < 160$ GeV) is the one which is expected to be enriched in t$\bar{\text{t}}$ events.
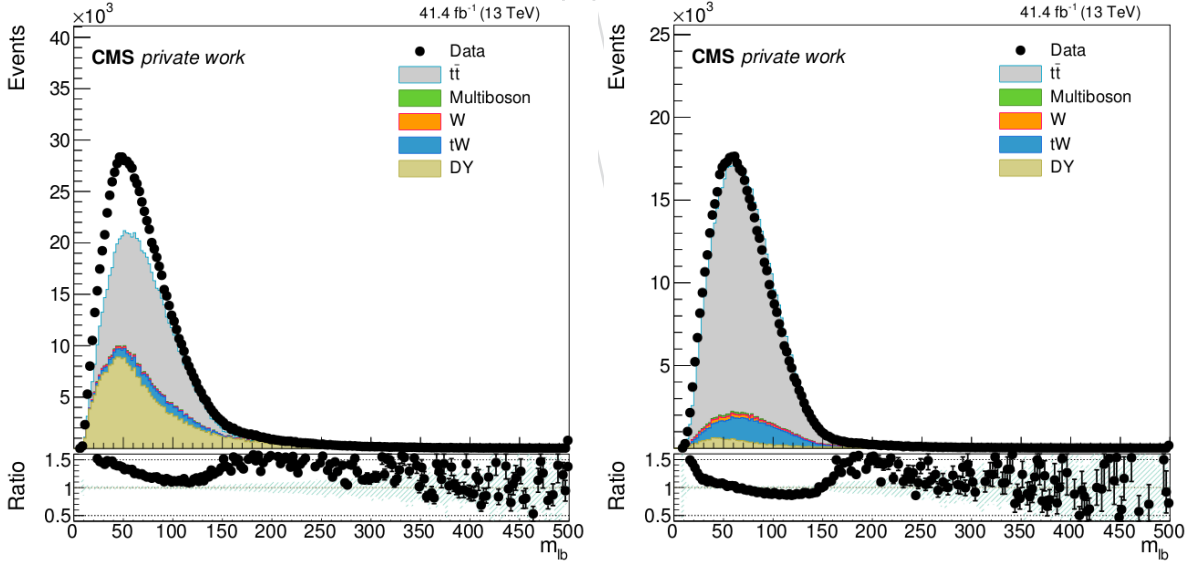

Figure 5: Control sample (central detector only): Mass of the lepton/b-jet system, after requiring two leptons, one jet and one b-jet, for same-flavour (SF) leptons in events outside the Z peak region (left), and for opposite-flavour (OF) leptons (right).

We compare exclusive (signal) and inclusive (background) t$\bar{\text{t}}$ samples with respect to specific variables reconstructed in the central detector. The variables are chosen as they are sensitive to the additional hadronic activity, which is expected to be suppressed in the case the production is exclusive and via electroweak vertices. The variables chosen are:

94 • $H_T = \sum_{j=1}^{N_j} |\vec{p}_{T,j}|$, the scalar sum of the transverse momentum of all jets except for the
95 b-jets;

96 • Hadronic recoil $h = |\vec{p}_T^{miss} + \vec{p}_T(\ell_1) + \vec{p}_T(\ell_2) + \sum_{j=1}^{N_b} \vec{p}_T(j)|$, obtained from the sum
97 of the missing transverse energy with the two charged leptons and up to two b-jets.
98 In the analysis we make use of the so-called puppiMET estimator for $\vec{p}_T^{miss}$ [11].

99 In the simulation, we observe that in the exclusive $t\bar{t}$ sample (signal) most of the events have
100 little "extra activity", that is most of the events have H_T=0 given there are no extra jets in the
101 events. In addition, exclusive $t\bar{t}$ events tend to have lower h when compared to inclusive $t\bar{t}$
102 production. Figure 6 shows the distributions of these variables in data and simulation. A slight
103 disagreement is observed with respect to the predictions, but no systematic uncertainties (e.g.
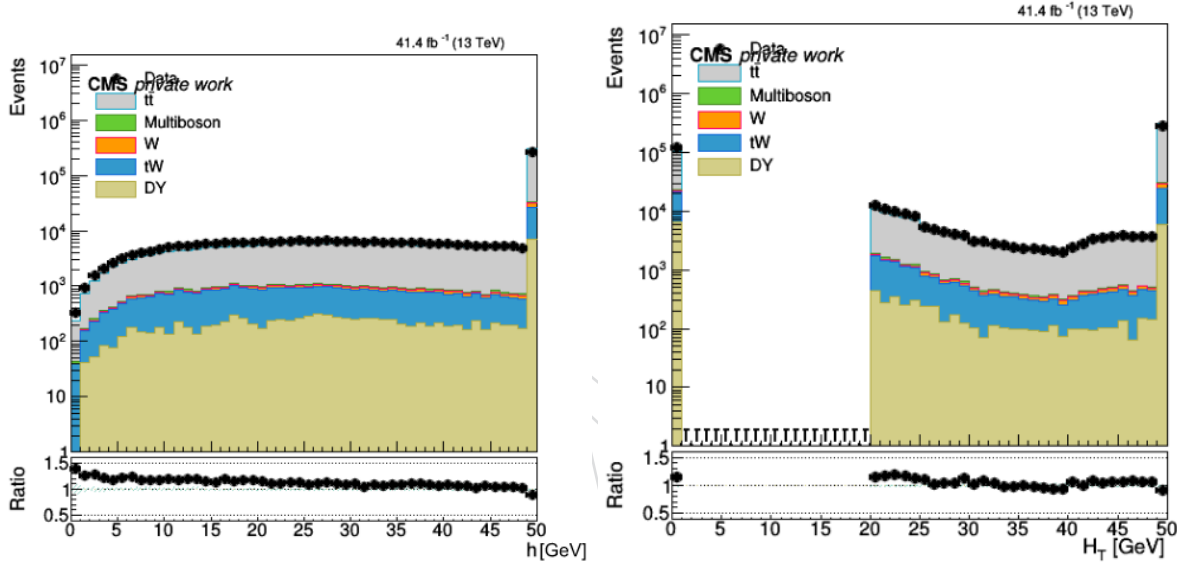104 related to pileup, and jet energy scale) are shown at this point.

Figure 6: Control sample (central detector only): Hadronic activity distributions obtained after requiring 2 opposite-flavour (OF) leptons, 1 jet, 1 b-jet, $m_{\ell b}$ <160 GeV. Distributions of the hadronic recoil h (left) and H_T (right) are shown (see text).

105 A comparison between distributions in exclusive (signal) and inclusive (background) $t\bar{t}$ events
106 is furthermore performed for the two important hadronic activity variables. Figure 7 shows
107 that the observed difference is significant between the two $t\bar{t}$ production mechanisms. This
108 information can be used to purify the event selection. In this analysis we require that $H_T = 0$
109 GeV in the signal region.

110 **3.2 PPS detector selection**

111 For the final selection, we use data from the pixel detectors. The choice for using the RP in-
112 strumented with the pixels is made as pixels can reconstruct more than one track per event
113 and, in case of pileup, the signal is not lost due to reconstruction inefficiency. For each track
114 reconstructed in the pixel detector it is possible to reconstruct the fractional proton momentum
115 loss (ξ). The ξ distribution for each pixel is shown in Fig. 8, for a fraction of the dataset.

116 From the values of ξ_0 (for z+) and ξ_1 (for z-) one reconstructs the mass and rapidity of the $t\bar{t}$
117 from the two protons in the RPs, using the following equations:
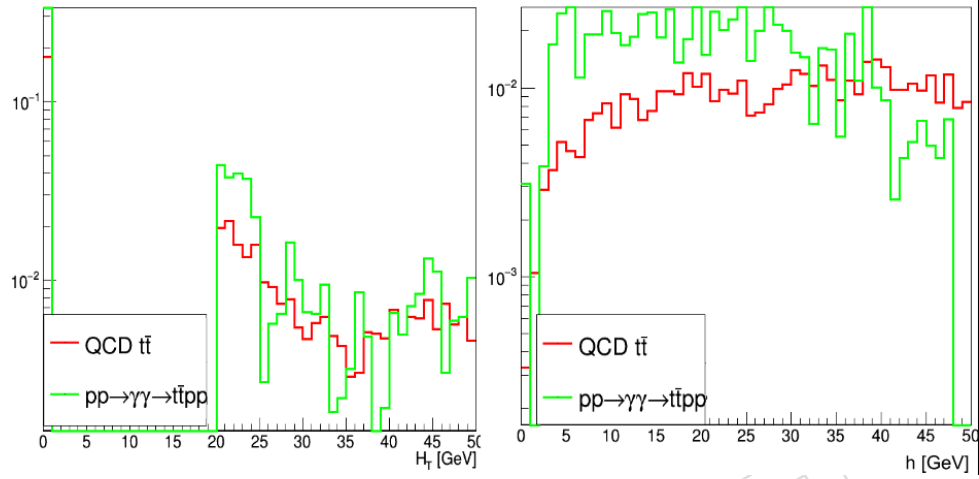
Figure 7: Control sample (central detector only): distributions of H_T (left) and h (right) for exclusive (signal) and inclusive (background) $t\bar{t}$ events. Distributions are normalized to unity.
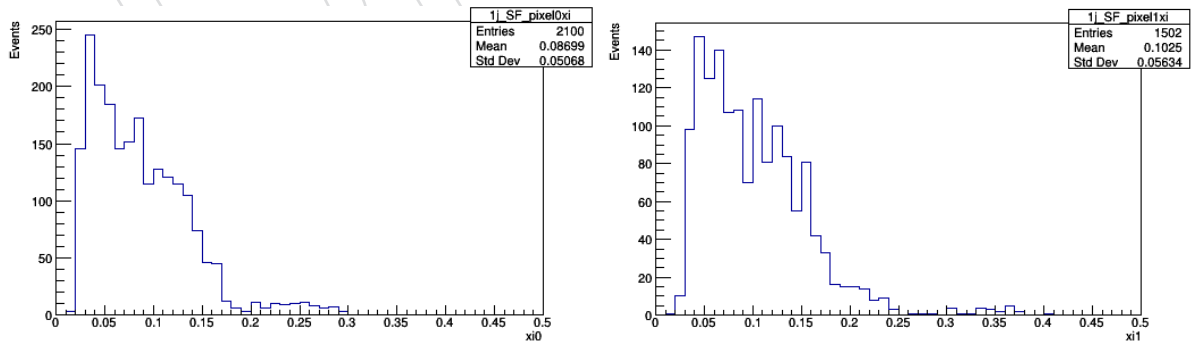

Figure 8: Distribution of the fractional momentum loss (ξ) of the protons detected in the pixels, for RP023 (left) and RP123 (right) (only a fraction of the dataset is used here).

$$m_{RP} = \sqrt{s \cdot \xi_0 \cdot \xi_1} \quad \text{and} \quad y_{RP} = \frac{1}{2} \ln \left(\frac{\xi_0}{\xi_1} \right),\tag{1}$$

where the subscripts 0 and 1 refer to the arm index.

Due to pileup (the average vertex multiplicity in the 2017 data is ~30), there is often more than one track per event in each pixel detector. Thus there is the need to reconstruct the mass and rapidity for every combination of tracks. Distributions of mass and rapidity are shown in Fig. 9 after requiring two leptons in the events.

Figure 9: Distributions of the reconstructed mass (left) and rapidity (right) of the dilepton system in the RPs, when requiring two opposite flavour (OF) leptons.
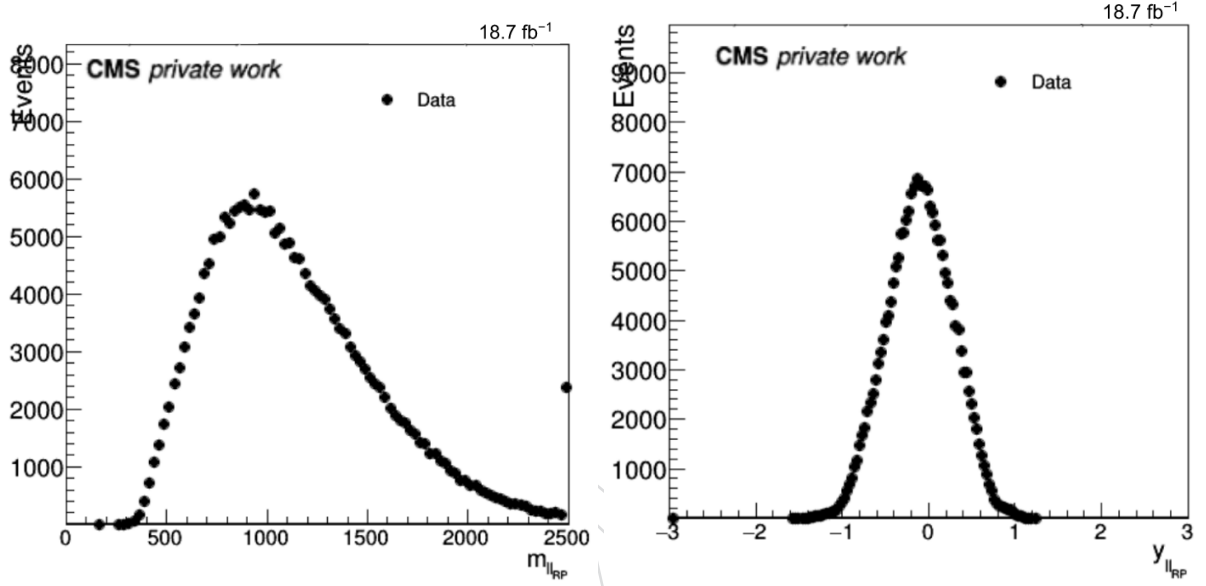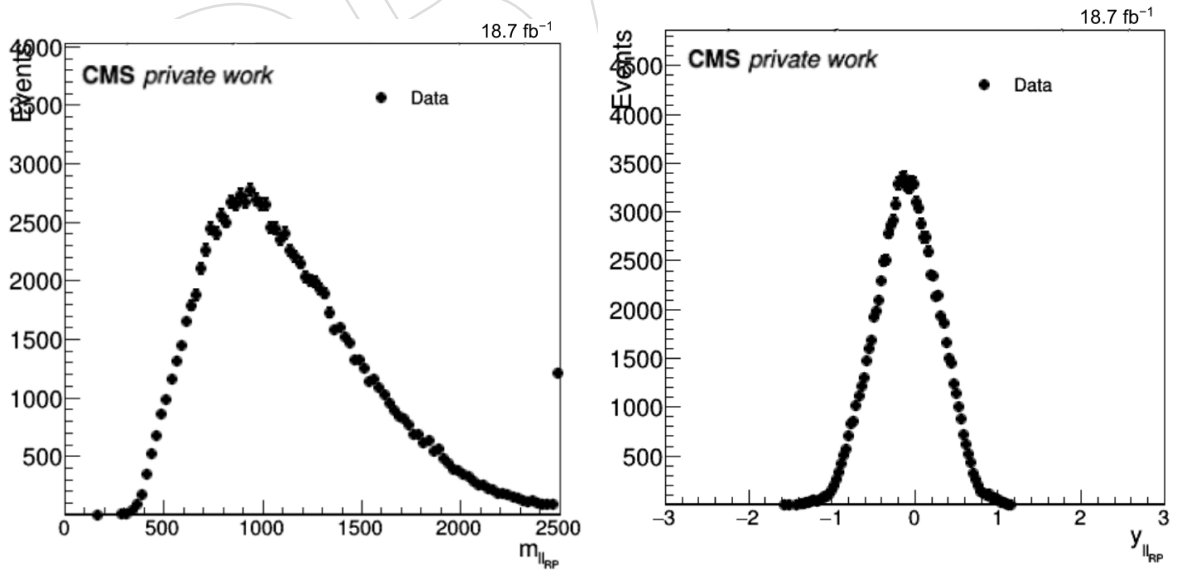

Figure 10: Distributions of the reconstructed mass (left) and rapidity (right) of the dilepton system in the RPs, when requiring 2 opposite-flavour (OF) leptons, 1 jet, 1 b-jet, low mass of the lepton/b-jet system ($M_{\ell b} < 160\,\text{GeV}$).

In this analysis, we select events in the $m_{RP} \in [300, 600]$ GeV range, chosen to be compatible with the bulk of the production threshold of exclusive $t\bar{t}$ events. Events are categorized depending on whether or not there is a combination of tracks that leads to a reconstructed $t\bar{t}$ mass in this range. This is discussed in the following Section.

3.3 Matching the central and the forward kinematics

A further improvement in the signal-to-background (S/B) ratio may be achieved by matching the kinematics of the events reconstructed in the central and in the PPS detectors. We apply the algorithm described in [12] to reconstruct the kinematics of the central system for the selected events. The algorithm is applied to the events which pass the full event selection described earlier. Given the ambiguity in the pairing of the leptons and the b-jets, and to the kinematics of the two outgoing neutrinos, up to 8 solutions can be found per event. We choose the solution that yields the lowest $m_{t\bar{t}}$. After this choice, the mass and rapidity values computed from the forward tracks are then compared with those reconstructed using the central system. The correlation between m_{RP} and y_{RP} is shown in Fig. 11. At this point no correlation is observed, i.e. the selected region is still largely dominated by inclusive $t\bar{t}$ events and pileup combinatorial background in the RPs. Figure 12 shows the same correlation for simulated exclusive $t\bar{t}$ events. We can see that for the rapidity the reconstruction performs quite well, and that is not the case for the correlation in the mass distributions.

4 Background determination

The most important background is due to non-exclusive $t\bar{t}$ events superimposed to random pileup protons reconstructed in PPS. This background is determined with a data-driven method. For this purpose, a combinatorial analysis is performed, where one takes the number of tracks per event and the ζ distributions in each pixel as observed at pre-selection level where the contribution from signal events is negligible. For each event, one generates a random number of tracks and a random ζ value for each of these tracks on each side of the PPS detector. This allows to reconstruct random pairs of tracks from where the mass and rapidity of the candidate combinatorial pp pairs can be computed. If one of these combinatorial pairs is found to have a mass within the $m_{RP} \in [300, 600]$ GeV range, the event is counted. Finally, the number of selected events is divided by the initial number of events in the sample, and the fraction of random coincidences is measured. We estimate the probability of random coincidences in this mass range to be $\approx 3.34\%$ with negligible statistical uncertainty. The result obtained is similar for the SF, OF, and Z peak categories.

This fake rate can be applied to all non-exclusive backgrounds and thus used to project the yields of non-exclusive $t\bar{t}$, tW, DY and dibosons in the signal region. There may be other subleading backgrounds that are not being considered, such as semi-exclusive $t\bar{t}$ events (where only one proton stays intact) with one pileup proton.

In addition, the events which do not pass the combinatorial pair selection (or the pair selection in data) are counted in separate categories that are used to normalize from data the initial estimates for $t\bar{t}$ and DY. The latter is normalized from SF events under the Z peak.

5 Determination of Roman Pot acceptance

In order to estimate the acceptance of the RPs for the exclusive $pp \rightarrow pt\bar{t}p$ signal, a sample generated with FPMC+Herwig is used. A 2-dimensional distribution comparing the mass and

Figure 11: Distributions of the mass (top) and rapidity (bottom) of the dilepton $t\bar{t}$ system as reconstructed using the algorithm in Ref. [12] (see text). 2D distributions are shown for the selected events reconstructed in the central detector (m_{cen}, y_{cen}) versus the values reconstructed from the RP tracks (m_{RP}, y_{RP}). The profile of each distribution is overlaid. The black cross centers at the mean and the bars indicate the standard deviation.
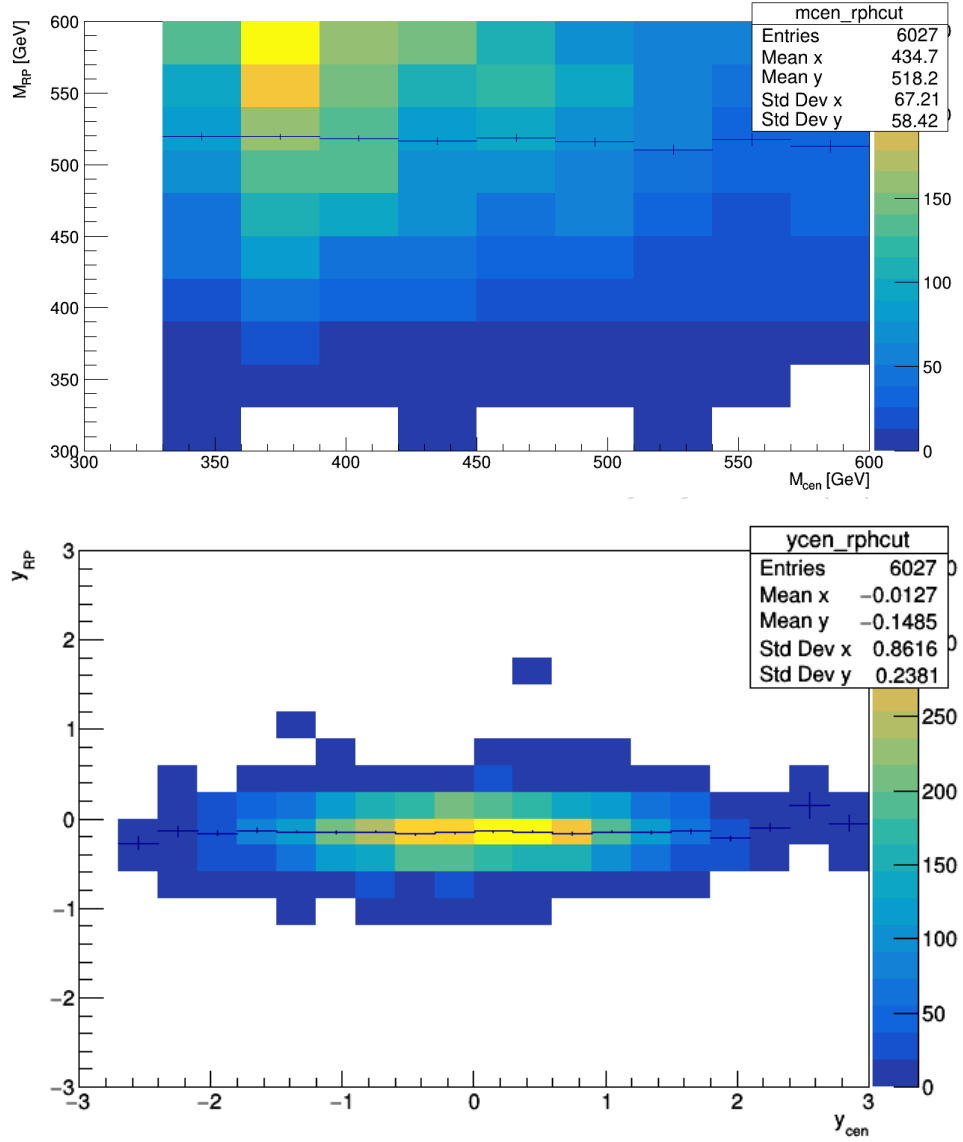
Figure 12: Distributions of the mass (top) and rapidity (bottom) of the dilepton $t\bar{t}$ system as reconstructed using the algorithm in Ref. [12] (see text). 2D distributions are shown for a sample of simulated exclusive $t\bar{t}$ events reconstructed in the central detector (m_{cen}, y_{cen}) versus the values reconstructed from the RP tracks (m_{RP}, y_{RP}). The profile of each distribution is overlaid. The black cross centers at the mean and the bars indicate the standard deviation.
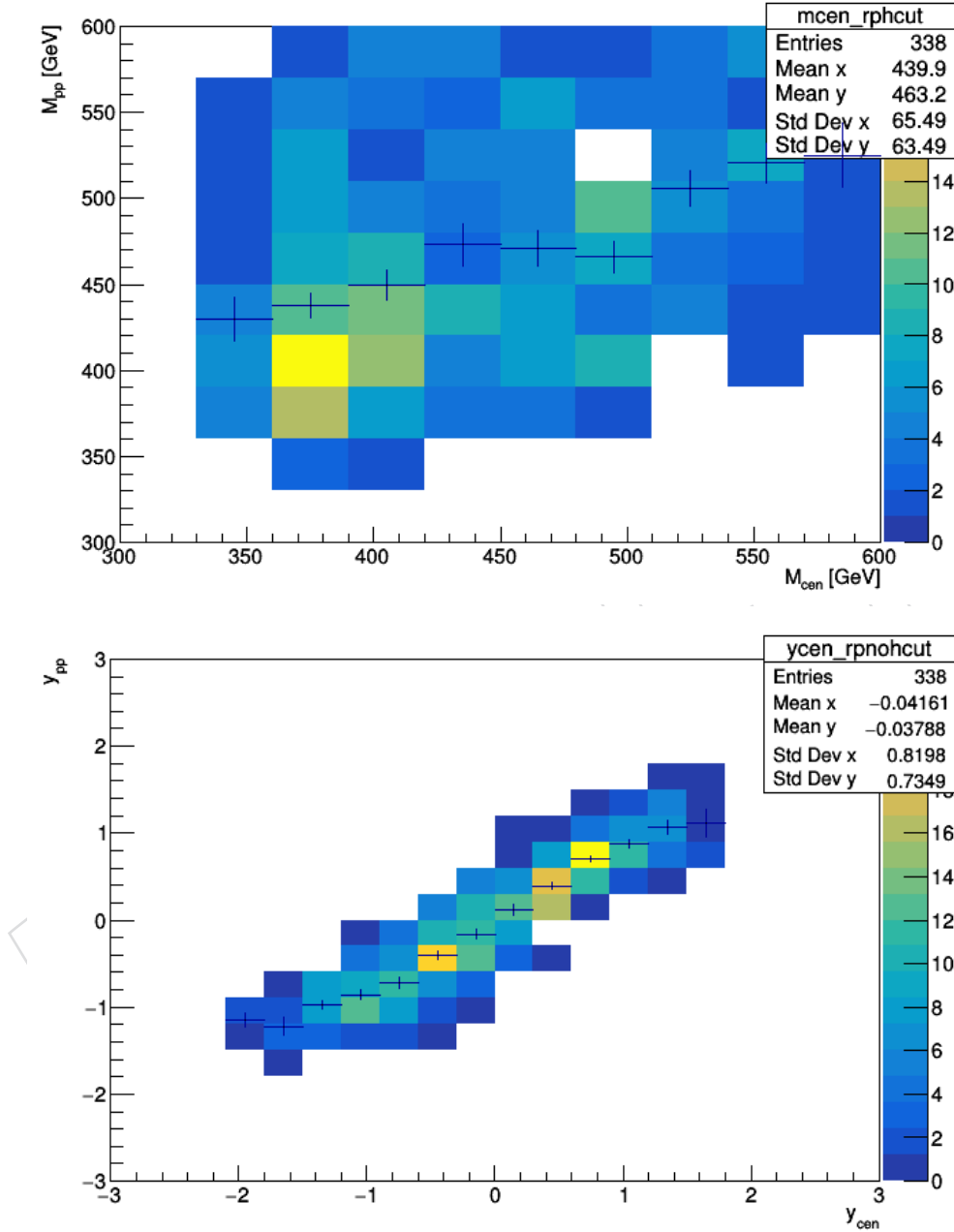
the rapidity of the simulated $t\bar{t}$ system is calculated, requiring two leptons in the final state. Then, a cut is applied by only selecting events that fall within the expected range of the RP acceptance, i.e. $0.02 < \xi < 0.2$. The distributions before and after the cut are shown in Fig. 13. From these plots, one simply divides the number of surviving events by the initial number of all simulated events. The acceptance of the RPs is measured to be 1.01%. This estimate is preliminary and could be further improved by considering that the RPs have an asymmetric acceptance between the two arms (see for example the ξ distributions in Fig. 8) and by taking the minimum and maximum values from the ξ distributions for each arm, instead of using a fixed expected range. However, the difference is not expected to be very significant.
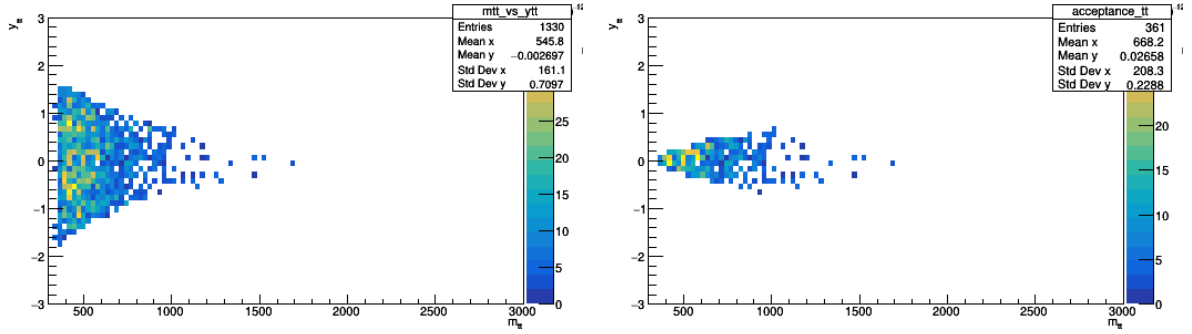

Figure 13: 2D distributions of the mass (m_{RP}) versus rapidity (y_{RP}) of the $t\bar{t}$ system in the signal sample, just requiring 2 leptons (left) and after requiring the tracks to be within the RP acceptance ($0.02 < \xi < 0.2$) (right).

selection step	surviving events	
Initial number of simulated events	35920	100%
Events with 2 leptons	1330	3.70%
Events in RP acceptance	361	1.01%

Table 3: RP acceptance: number of events surviving the selection cuts and their corresponding fractions.

6 Determination of $\sigma(pp \rightarrow pp2\ell1b)$ through a statistical analysis

The final event yields, including the extrapolation of the backgrounds in the signal region using the fake rate method described in Sec. 4, are shown in Table 4. The 5 different categories share in common the selection of:

- ≥ 2 leptons with $m_{\ell\ell} > 20\,\text{GeV}$;
- ≥ 1 b-jet;
- $m_{\ell b} < 160\,\text{GeV}$.

The specific requirements of the final event categories are the following:

SR_OF - $e\mu$ events with $m_{RP} \in [300, 600]$ GeV and $H_T = 0\,\text{GeV}$;

SR_SF - similar to SR_OF, but for same-flavour events outside the Z peak;

$t\bar{t}$ **CR_OF** - $e\mu$ events failing the $m_{RP} \in [300, 600]$ GeV cut;

$t\bar{t}$ **CR_SF** - similar to $t\bar{t}$ CR_OF, but for same-flavour events outside the Z peak;

186 **dyCR** - similar to t$\bar{\text{t}}$ CR_SF, but for same-flavour events inside the Z peak.

187 In the following, we perform a combined fit of the event yields observed in each category.

Process	SR_SF	SR_OF
inclusive t$\bar{\text{t}}$	1172	1460
DY	1742	97
others	30	34
total	2944	1591
data	2538	1130

Table 4: Yields in the signal region for different background contributions and for those observed in data.

Process	t$\bar{\text{t}}$ CR_SF	t$\bar{\text{t}}$ CR_OF	dyCR
inclusive t$\bar{\text{t}}$	**415937**	**519492**	114783
DY	271583	17395	**2863390**
others	9962	12180	11756
total	697483	549068	2989929
data	903621	550805	3759454

Table 5: Yields in the control regions for different background contributions and those observed in data.

188 6.1 Method employed in the statistical analysis

189 The number of events observed in the signal and control regions can be analyzed to set limits
190 on the production cross section of $pp \to pp2\ell1b$. In order to do it we parametrize the total
191 number of events expected in a single category as follows:

$$N_{\text{exp}} = N_{\text{exp}}(pp \to pp2\ell1b) + f \cdot \left[N_{\text{exp}}(t\bar{t}) + N_{\text{exp}}(tW) + N_{\text{exp}}(DY) + N_{\text{exp}}(\text{others}) \right] \quad (2)$$

192 where f is the probability that a non-exclusive event passes the selection of the RPs due to
193 combinatorial tracks. In Eq. 2 we assume that there is no additional exclusive process which
194 may contribute in the selected regions. The CRs for t$\bar{\text{t}}$ and DY are used to normalized the
195 initial expectations based on simulation. We thus employ $\mu_{t\bar{t}}$ (μ_{DY}) as scaling factors of the
196 initial expectations for t$\bar{\text{t}}$ (DY), i.e.:

$$N_{\text{exp}}(b) = \mu_b \cdot N_{\text{exp}}^{\text{MC}}(b) \quad (3)$$

197 where b=t$\bar{\text{t}}$,DY and $N_{\text{exp}}^{\text{MC}}(b)$ is the expectation from simulation which includes the theory cross
198 section, the integrated luminosity, and the corrections for the simulated efficiency with data-
199 to-MC scale factors. Other processes in Eq. 2 will float constrained according to the estimated
200 uncertainties. The expectations for the signal are written as a product of the following factors:

$$N_{\text{exp,c}}(pp \to pp2\ell1b) = A \cdot L \cdot \varepsilon_{\text{c}} \cdot \sigma(pp \to pp2\ell1b) \quad (4)$$

201 where c=SF,OF is the event category, A is the acceptance at generator level for the selection of
202 two leptons and an invariant mass of the outgoing protons in the PPS detector acceptance, L

is the total integrated luminosity, ε_c is the selection efficiency, and $\sigma_p p \rightarrow pp2\ell1b$ is the cross section. Given that the selection criteria differ slightly in the SF and OF categories, the efficiency factors in Eq. 4 are computed separately for each category. With these definitions in hand, we can maximize the following likelihood as function of $\sigma_p p \rightarrow pp2\ell1b$

$$\mathcal{L} = \prod_{k=1}^{N} \mathcal{P}_{\text{oisson}}(N_{\text{obs}}|N_{\text{exp}}) \cdot \prod_{m=1}^{M} f(\theta_k) \tag{5}$$

where the first product runs over the N categories in which events are counted, and the second product runs over M nuisance parameters which encode the relative uncertainty of the parameters employed to parametrize the expectations N_{exp}. The PDF $f(\theta_k)$ is taken as a log-normal function. The implementation of Eqs 2- 5 is made in RooStats, using the Higgs Combine Tool.

6.2   Summary of the inputs to the statistical analysis

Table 6 summarizes the values used for the acceptance, efficiency, and the number of expected events corresponding to the integrated luminosity in which the data are analysed. The systematic uncertainties considered in the fit are listed in Table 7.

	SF	OF
Signal acceptance	0.0101	
Selection efficiency ($m_{\ell b} < 160\,\text{GeV}$)	0.345	0.428
N (luminosity * acc. * eff.)	65.055	80.697

Table 6: Summary of the inputs to the statistical analysis. Signal acceptance, the selection efficiency in the signal region ($m_{\ell b} < 160\,\text{GeV}$), and the number of expected events. Numbers are shown for same-flavour (SF) and opposite-flavour (OF) categories.

Uncertainty	Value	It affects
Luminosity	2.7%	all processes
$\sigma_{\text{inclusive } t\bar{t}}$	5.1%	inclusive $t\bar{t}$ (SR and CR)
σ_{others}	30%	others
DY uncertainty	30%	Drell-Yan
Fake rate	5%	all processes except signal
Lepton selection efficiency	3%	all processes

Table 7: Systematic uncertainties used in the analysis.

6.3   Results

Using the Higgs Combine Tool with the inputs listed in Section 6.2, one can obtain the likelihood plots shown in Fig. 14. It is then possible to get an asymptotic upper limit on the exclusive $t\bar{t}$ cross section: $\sigma < 900^{+360}_{-253}$ fb (68% confidence level), or 900^{+415}_{-788} fb (95% confidence level).

7   Conclusions

We analysed the 2017 data searching for exclusive $t\bar{t}$ production in the dilepton final state. An inclusive selection for two leptons and at least one b jet is studied and the background estimated. Signal discrimination variables are studied based on a dedicated simulation of $pp \rightarrow p\gamma\gamma p \rightarrow pt\bar{t}p$. The estimated upper limit on the production cross section of exclusive $t\bar{t}$ production is 900 fb.
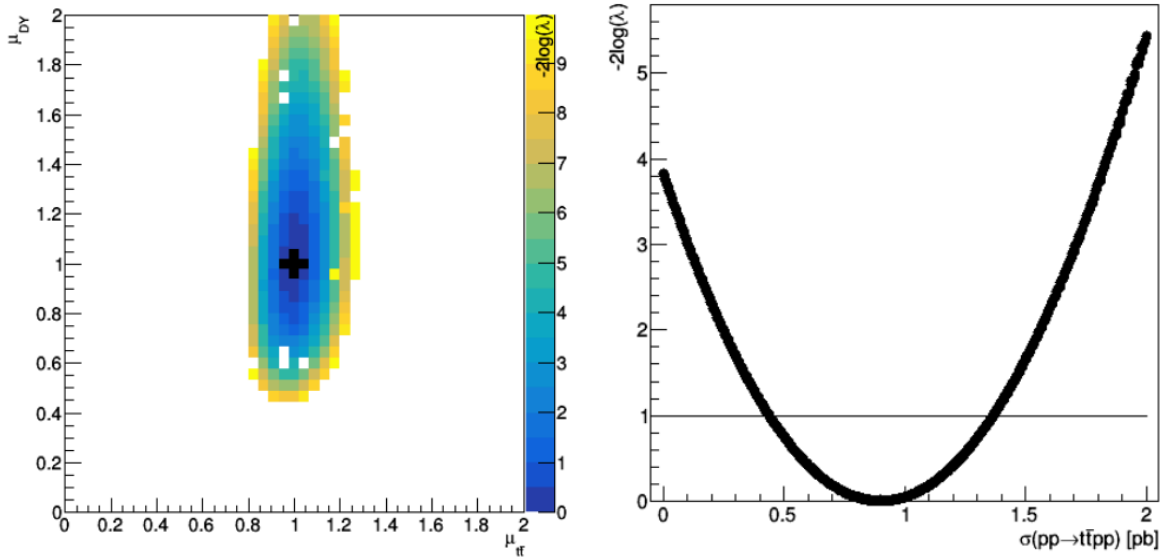
Figure 14: *Left:* Contour of the likelihood for the scale factors for inclusive $t\bar{t}$ ($\mu_{t\bar{t}}$) and DY (μ_{DY}) processes fitted using dedicated control regions. The black cross marks the fitted values. *Right:* Likelihood scan results for the expected signal for a cross section of $\sigma = 900$ fb. The line intersects the likelihood at the boundaries of the 68%CL.

References

[1] J. de Favereau de Jeneret et al., "High energy photon interactions at the LHC", `arXiv:0908.2020`.

[2] P. J. Bussey, T. D. Coughlin, J. R. Forshaw, and A. D. Pilkington, "Central exclusive production of longlived gluinos at the LHC", *JHEP* **11** (2006) 027, `doi:10.1088/1126-6708/2006/11/027`, `arXiv:hep-ph/0607264`.

[3] S. Heinemeyer et al., "Central Exclusive Production of BSM Higgs bosons at the LHC", in *Proceedings, 38th International Symposium on Multiparticle Dynamics (ISMD 2008): Hamburg, Germany, September 15-20, 2008*, pp. 338–343. 2009. `arXiv:0811.4571`. `doi:10.3204/DESY-PROC-2009-01/60`.

[4] S. Taheri Monfared and S. Fayazbakhsh, "Probing Anomalous Top Quark Couplings in Diffractive Events at the LHC", *Acta Phys. Polon. Supp.* **7** (2014), no. 3, 579, `doi:10.5506/APhysPolBSupp.7.579`.

[5] K. Piotrzkowski and N. Schul, "Two-photon exclusive production of supersymmetric pairs at the LHC", *AIP Conf. Proc.* **1200** (2010) 434–437, `doi:10.1063/1.3327609`, `arXiv:0910.0202`.

[6] M. Boonekamp et al., "FPMC: A Generator for forward physics", `arXiv:1102.2531`.

[7] M. Bahr et al., "Herwig++ Physics and Manual", *Eur. Phys. J. C* **58** (2008) 639–707, `doi:10.1140/epjc/s10052-008-0798-9`, `arXiv:0803.0883`.

[8] JME group Collaboration, "Jet identification in high pile-up environment ", twiki, 2017.

[9] CMS Collaboration, "Identification of heavy-flavour jets with the CMS detector in pp collisions at 13 TeV", *JINST* **13** (2018), no. 05, P05011, `doi:10.1088/1748-0221/13/05/P05011`, `arXiv:1712.07158`.

248 [10] Particle Data Group Collaboration, "Review of Particle Physics", *Phys. Rev. D* **98** (2018),
249   no. 3, 030001, `doi:10.1103/PhysRevD.98.030001`.

250 [11] CMS Collaboration, "Performance of missing transverse momentum in pp collisions at
251       $\sqrt{s} = 13$ TeV using the CMS detector", Technical Report CMS-PAS-JME-17-001, CERN,
252   Geneva, 2018.

253 [12] B. A. Betchart, R. Demina, and A. Harel, "Analytic solutions for neutrino momenta in
254   decay of top quarks", `doi:10.1016/j.nima.2013.10.039`,
255   `arXiv:arXiv:1305.1878`.